



# Modelling of non-structural components of an industrial multi-storey frame for seismic risk assessment

Gianluca Quinci<sup>1</sup> · Chiara Nardin<sup>2</sup> · Fabrizio Paolacci<sup>1</sup>  · Oreste S. Bursi<sup>2</sup>

Received: 23 February 2023 / Accepted: 31 July 2023 / Published online: 7 September 2023  
© The Author(s) 2023

## Abstract

Seismic risk assessment of industrial facilities is complex due to the presence of different types of equipment. It represents a research issue that requires further investigation. To this end, some analytical approaches have been developed in the framework of performance-based earthquake engineering. Nonetheless, their accuracy in the case of complex critical facilities, such as nuclear and non-nuclear industrial plants, is still under investigation. Thus, the proposed study intends to research in depth, in a risk assessment framework, some critical aspects related to: (1) modelling of industrial facilities and their secondary equipment with different degrees of accuracy, also taking into account their dynamic interaction; (2) selection of seismic records for fragility analysis, due to the narrow distribution of frequency values for non-structural components; (3) effectiveness of performance-based earthquake engineering applied to this particular class of coupled structure-equipment for risk assessment. In this context, the proper selection of seismic records becomes relevant, and SCoRes, an innovative algorithm for accelerograms selection is worthy of investigation. On these premises, two different configurations of a primary industrial structure, i.e. a moment resisting frame and a braced frame, equipped with non-structural components and subjected to shake table test campaigns are selected as case studies. For the two configurations, a vulnerability assessment of two vertical tanks installed on the first floor was carried out. Along these lines, to establish the effectiveness of the proposed method for both the moment resisting frame and braced frame configurations, the mean annual frequency of exceedance of the bottom-wall strain of the above-mentioned tanks, both at the design basis and safe shutdown earthquake has been evaluated.

**Keywords** Industrial facilities · Non-structural component · Record selection · FE modeling · Computational burden · Fragility curves · Risk assessment

## 1 Introduction

### 1.1 Background and motivation

The seismic behaviour of support structures in major-hazard industrial plants, e.g. chemical facilities, refineries, etc. is of paramount importance as undoubtedly demonstrated by many

---

Extended author information available on the last page of the article

contributions present in the literature. Several researchers, indeed, analyzed the main issues concerning both the modelling and component design of industrial plant substructures equipped with process equipment, e.g. pipes, tanks, tee-joints, etc. (Caputo et al. 2019). Notwithstanding, several aspects are still unresolved, and this result in codes and standards often dated and inadequate, especially with regard to consequences on humans, the environment and recent approaches such as the PBEE (Bertero and Bertero 2002). For instance, De Angelis et al. (2010) came to the conclusion that both European (European Committee for Standardization 2011) and American (American Society of Mechanical Engineering 2000) standards provide limited indications for assessing the seismic response of refinery piping systems, where support rack structures and components, e.g. pipes, flange joints, etc. are present. In particular, an allowable stress design approach is preferred, even though modern literature suggests a PBEE approach.

The main obstacle to the widespread adoption of PBEE is the need for accurate nonlinear models, which are computationally expensive and require specific and high-standard skills. A few studies can be found in the literature where an explicit PBEE approach has been used for the seismic analysis of these special structures. For instance, in Bursi et al. (2016), the application of the PBEE approach is illustrated through complete nonlinear seismic analyses of two petrochemical piping systems. The authors concluded that a general overconservatism in designing piping systems is typically adopted, even though it is neither economic nor advanced. Needless to say that, given the scarcity of experimental data, the definition of performance parameters and limit states has a certain degree of complexity. Zito et al. (2022) represents an interesting state of the art of testing approaches and protocols for the seismic assessment of NSCs by means of experimental methods. An interesting attempt to rationalise this aspect with regards to storage tanks under seismic loading can be found in Butenweg et al. (2021); however, the lack of experimental results on the local behaviour of industrial components still represents a critical aspect on which limited contributions are present in the literature (Butenweg et al. 2021). Along this main vein, a significant contribution was provided by the SPIF experimental campaigns, Nardin et al. (2022) and (Reza et al. (2014)), where two different—MRF and BF—substructure configurations equipped with pipes and tanks have been tested through a shaking table test campaign and the local behaviour of NSCs have been deeply analyzed. Furthermore in Bursi et al. (2016), the authors investigated the behaviour of non-standard bolted flange joints endowed with plastic deformation capacity, demonstrating that entering into the inelastic regime in case of strong earthquakes can be beneficial in terms of dissipation, even in the presence of potential release of hazardous materials. Moreover, to investigate the performance of a full-scale petrochemical piping system under strong motions, Sayginer et al. (2020) used the hybrid testing techniques; they demonstrated that the piping system, which was designed according to the current codes, exhibited a clear overstrength. Along these lines, the identification of suitable nonlinear analysis methods for properly evaluating limit states exceeding defined threshold represents another significant issue.

One of the most reliable analysis methods, in order to take in account the nonlinear behaviour of both primary structures and secondary elements is the dynamic integration of the system of equation of motion (SOM). Despite the reliability of the aforementioned method, usually simplified approaches, such as the use of floor spectra or static analysis are preferred; nonetheless these latter are not problem-free. In this respect, (ASCE/SEI 2016) demonstrated that the standard nonlinear static analysis cannot be used to assess a piperack response and that the current behaviour factor used in the standards is not adequate. The reason realises in the fact that this kind

of structures show some non-building characteristics, such as the coupling effects between primary and secondary structures and the absence of rigid floor, that lead to these discrepancies (Merino Vela et al. 2018). Another crucial point consists in the method used for the analyses. For example, an analysis based on floor acceleration spectra is carried out in Calvi and Sullivan (2014) to evaluate the responses of a liquid storage tank installed on an industrial concentrically braced frame (CBF) structure. The authors clearly demonstrated a general over conservatism of the approaches provided by the codes in respect of analyses that explicitly take into account the interaction between the supporting structure and the installed equipment. A practical approach for the derivation of floor spectra has been proposed by Caputo et al. (2020), where simplified formulas for SDOF and MDOF models were proposed, which can accurately predict peak spectral quantities. These approaches were successfully adopted by Calvi and Sullivan (2014) to estimate floor spectra for an industrial CBF structure, accounting for nonlinearities.

Special attention should also be paid to the consequences that a failure of supported components, e.g. pipe flanges and elbows, tanks, etc., can induce on humans and the environment. Caputo et al. (2020) analysed the problem in view of a quantitative seismic risk analysis (QRA) of major-hazard process plants. They highlighted that one of the critical points that caused a limited diffusion of QRA was due to limited knowledge of the seismic behaviour of critical units and components, among which the support structures play a crucial role. Release of hazardous materials from secondary elements, e.g. pipes, tanks, etc., even not directly considered by the current standards, could generate serious damages, dramatically amplified by domino effects (Alessandri et al. 2018). Its relation with seismic damage represents the main problem in the evaluation of loss of containment (LOC), which is still under investigation (Merino et al. 2019). Therefore, the need for additional data provided by experimental campaigns on realistic support structures with NSCs subjected to seismic loading is evident. Moreover, an additional open issue is represented by a proper definition of limit states and related seismic action demands. Whilst seismic hazard levels and structural limit states -including consequences- are clearly identified for civil buildings, little information can be found for hazardous industrial equipment and support structures. An initial attempt to analyse the consolidated approaches of the nuclear industry in an industrial facility setting can be found in Di Sarno and Karagiannakis (2020); more precisely, a typical coupled support structure-refinery piping system was analysed referring to both design basis (DBE) and safe shutdown earthquakes (SSE). The first earthquake level corresponds to typical safe life limit state conditions, whereas the second level is related to near collapse conditions. Nevertheless, these results should be extended to other types of structural configurations coupled with process equipment. Along this vein in Reza et al. (2014), the authors identified limit state performances and related thresholds for industrial pipes, tanks and support structures based on experimental results and engineering evaluations.

From the above-mentioned considerations, it is evident that a number of unresolved issues deserve investigation, which is mainly related to lack of data in the nonlinear regime. Furthermore, a few contributions relevant to the seismic risk assessment of NSCs can be found in the literature (Giannini et al. 2022). In this direction, to study the dynamic interactions of both the support structure and the NSCs, the SPIF projects were conceived to partially fill the paucity of data by testing a full-scale industrial plant substructure equipped with process components under realistic seismic conditions (Nardin et al. 2022; Reza et al. 2014).

## 1.2 Scope

In summary, to perform a reliable risk assessment of process equipment, the following objectives are pursued hereinafter: (1) the conception and development of simple yet reliable FE models of critical NCSs coupled to representative support structures; (2) the selection of seismic records for the evaluation of the mean annual frequency (MAF) of exceedance of the bottom-wall strain of two vertical tanks, both at the DBE and SSE levels. In particular, efficient and reliable FE models that balance the computational burden and complexity required for a fragility analysis are set. Successively, the seismic risk assessment of two typical industrial NSCs, represented by vertical tanks located at the first level of a three-storey support structure is carried out; to this end, an innovative methodology for the stochastic selection of seismic records using the algorithm ScoReS proposed by the authors in Butenweg et al. (2020) is employed.

The rest of the paper is organized as follows. Firstly, Sect. 2 provides a brief overview of the SPIF projects and their main results. Then, both Sects. 3 and 4 present an overview of the modelling issues encountered, the relevant solutions proposed and the FE models calibration and validation. Section 5 instead, presents the seismic risk assessment framework and the application to the two NSCs involved in the case studies. Finally, Sect. 6 draws conclusions and future developments.

## 2 Description of the case studies

Within the European research framework Horizon2020, the SPIF projects, i.e. *Seismic Performance of Multi-Component Systems in Special Risk Industrial Facilities*, was conceived and realized through extensive shaking table test campaigns on real scale industrial archetype substructures (SAP2000-v22 2022). More precisely, the objectives of the SPIF projects were the investigation of the dynamic interaction between the main steel structure and the installed process components or non-structural components (NSCs) in a performance-based earthquake perspective as well as the evaluation of the seismic performances of the two most widespread design configuration for industrial plants. The two different configurations, i.e. the moment resistant frame (MRF) and the braced frame (BF), were tested by a uniaxial shaking table with several PGA's levels of a scaled spectrum-compatible record and a synthetic ground motions *ad-hoc* selected for the experimental campaign, reaching the final intensity of 0.71 g and 0.79 g, respectively. An interested reader may find more information on the seismic input selection and the carried out test programme in Nardin et al. (2022) for the MRF configuration and (Reza et al. 2014) for the BF.

Figure 1a–d shows the specimen tested by means of a shaking table. The primary steel structure consists in a three-level frame equipped with vertical and horizontal tanks, piping system and several bolted flange joints (BFJs). The floor dimensions are 3.7 m × 3.7 m, while the total height of the specimen is 9.3 m, i.e. 3.1 m for each storey. According to the tested configuration, the load-bearing system consists in two MRFs or BFs in the seismic input direction, while in the transversal direction two braced frame made by a circular cross-section were installed for both the configurations. No rigid floors are present in the specimens as usually happens in this kind of structures and the secondary frame beams



**Fig. 1** Photos of the SPIF's mock-up tested in EUCENTRE lab, Pavia, Italy: **a** the MRF configuration; **b** the two installed vertical tanks; **c** details of the BFJ between the vertical tank and the piping system at 1st level; **d** the BF configuration

are connected to the main frame beams by simple bolted connections with web stiffeners. The crossbeams system served as bearing supports for installing the NSCs. More precisely, two vertical tanks, i.e. Tank #1 and #2, were installed on the first floor and two horizontal tanks, i.e. Tank #3 and #4, were located at second floor, as depicted in Fig. 1a–d. Furthermore, all the tanks were filled with a granular material with a density equal to water with the aim on one hand to simulate the liquid typically stored in such tanks and on the other hand to protect the shaking table against liquid release. Finally, a piping system consisting of nine DN100 pipes, with a 100 mm diameter and a 3.6 mm thickness, was installed on the specimen in order to connect tanks with each other and tanks with the ground. The piping system is made by straight branches, elbows, BFJs and tee joints. S235 with a yield strength of 235 N/mm<sup>2</sup> is the steel used for both tanks and piping system.

Testing results demonstrated a clear, dynamic interaction between the primary steel structure and the secondary process components in both configurations.

More precisely, in the MRF case, the primary steel structure remained undamaged for safe shutdown earthquake (SSE) levels mainly due to its design and inherent flexibility; whilst in the BF case, the main structure exhibited almost a linear behaviour until the foreseen buckling of the bracing system. However, due to the use of common practice solutions for NSC components, damage appeared in web plates of fin plate connections for main members and supporting floor crossbeams at the first level. In fact, due to the intense rocking of the vertical tanks #1 and #2, fin plate connections experienced warping of the crossbeam's web and cracks in the transition zone from beam to web.

Concerning the NSCs performances, leakage phenomena at the monitored BFJs did not occur, as predicted by analytical formulations based on design codes, in any of the MRF and BF cases. Moreover, the vertical tanks at the first level experienced intense rocking in both MRF and BF configurations. Conversely, in terms of interactions with the main structure, they resulted in a different seismic performance. Owing to dynamic properties,

in the BF configuration, the vertical tanks acted as tuned mass dampers (TMDs), and thus the relevant base shear at the first floor was limited; instead, in the MRF configuration, the favourable TMD effect was not relevant, as collected data and further studies revealed. Overall, it was shown that a proper experimental test campaign could: (1) highlight complex interactions and potential damage in industrial substructures; (2) reveal the efficiency of different system configurations.

### 3 Multi-storey frame and equipment modelling issues

To better understand the complex dynamics of the system, FE models of SPIF mock-ups were deemed necessary. The rationale behind developing these models was to gain the optimal balance between computational demand time and reliability in assessing SPIF's experimental campaigns.

To do so, global models for the MRF and BF configurations, calibrated on local parametric analyses on the critical components, e.g. bolted flange joints (BFJs), pipes, tanks, etc., of those special-risk facilities, were implemented in SAP2000 software (European Committee for Standardization 2004). In particular, the following components were the object of a thorough, in-depth investigation: (1) for the main structure—base joints and fin plates connections; (2) for the piping system- elbows and BFJs; (3) for NSCs—vertical and horizontal tanks (Fig. 2).

#### 3.1 Main steel frame structure

For the modelling of both MRF and BF configurations, linear elastic elements have generally been adopted. Along this vein, columns and beams have been modelled by

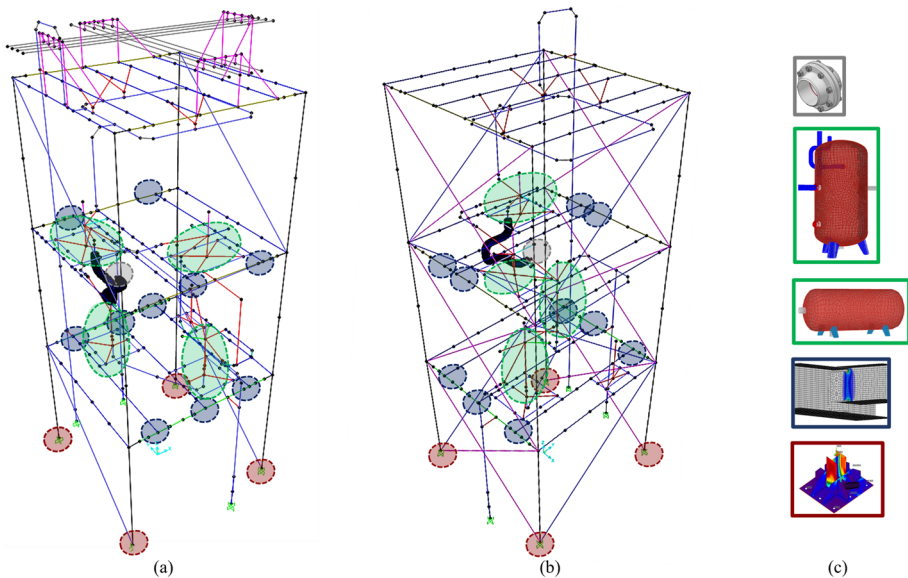


**Fig. 2** FE global models in SAP2000<sup>®</sup>: **a** the global MRF model; **b** the global BF model; **c** local HF models and their locations in **(a)** and **(b)**

Euler–Bernoulli elements. Furthermore, in order to correctly simulate the flexible behaviour of the floors, no-rigid diaphragms were applied at various levels. A Young's modulus of 220 GPa was assumed for the steel primary structures, following the results of the model updating procedure described in detail in Sect. 4.1.

Thus, thanks to the rational fraction polynomials (RFPs) identification technique applied to the gathered data of the experimental campaigns, a damping ratio of 4.5% was introduced as suggested by the European (U.S. Nuclear Regulatory Commission 2007) and nuclear standards (IDEA 2022). Further information on system identification can be found in Nardin et al. (2022) and (Reza et al. 2014). Moreover, as testing results demonstrated, fin plate connections between main members and secondary beams were critical seismic details. Therefore, to reproduce the dynamic of the shaking table test campaigns and calibrate the moment-rotation relationship for local flexural plastic hinges, a component-based finite element model (CBFEM) analysis of the detail was carried out with the software IdeaStatica (European Committee for Standardization (2005).

Results of the CBFEM analysis confirm severe stresses and significant strain levels in correspondence with the fin plate notch in the exact location where they were recorded during the experimental campaign. Figure 3a highlights strain values exceeding 12‰ yield threshold, thus explaining cracks initiation and propagation photographed in Fig. 3b.

The moment-rotation curve evaluated by European Committee for Standardization (2005) was then applied to the flexural plastic hinge definition in SAP2000.

Furthermore, due to its complexity and relevance to the global response of the SAP2000 models, also base joint connections were thoroughly examined by referring to a CBFEM developed within IdeaStatica (European Committee for Standardization 2005). Therefore, the rotational joint stiffness  $S_{j,ini}$  of the column base was derived, as reported in Fig. 4a. Moreover, as reported in the graph, following §5.2.2.5(2) of EN 1993–1-8 (Vathi et al. 2017), it was evaluated  $S_{threshold} = 109.4 \text{ MNm/rad}$ , through Eq. (5.2d) that discriminates between rigid and semi-rigid joints. As  $S_{j,ini}/S_{threshold} = 0.21$ , we clearly deal with a semirigid and partial strength base joint. Thus, it was possible to derive the equivalent rotational stiffness to apply to the base joint rotational link  $k = S_{j,ini} L_c / EI_c$ .

Finally, for the BF configuration, additional non-linearities were introduced to model the bracing system through nonlinear tension-only elements.

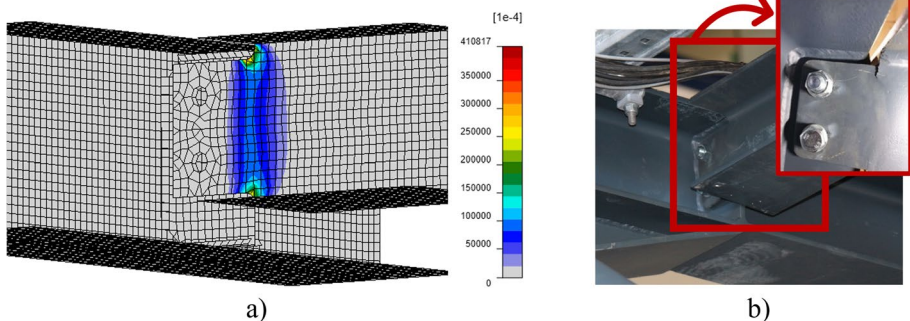


**Fig. 3** Thin plate: **a** CBFEM strain analysis results; **b** photos of the crack initiation on the mock-up

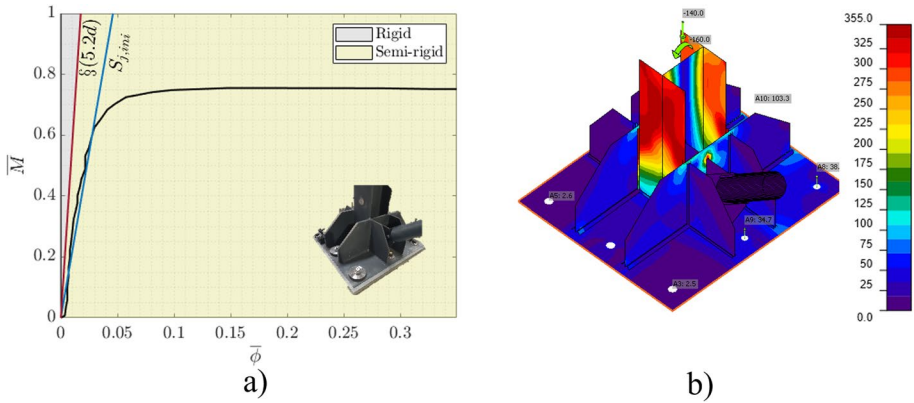


**Fig. 4** Base joint: **a** semi-rigid joint classification, according to §5.2.2.5(2) of EN 1993-1-8 (Vathi et al. 2017); **b** CBFEM of IDEA StatiCa® stress analysis results

### 3.2 Piping systems and non-structural components

A parametric analysis was carried out with respect to the NSCs, such as piping system and tanks, in order to reduce the computational burden required by the analysis.

Several techniques can be found in literature in order to model the inherent stiffness and flexibility of piping system, see among others (Kireev and Berkovsky 2013).

Flexibility factors were adopted herein for modelling tee-joints and straight pipes through beam elements with a reduced stiffness, following the suggestions provided in European Committee for Standardization (2011). With respect to the elbows, instead, that are highly susceptible to ovalization and warping effects, straight beam elements were adopted when it was possible to ensure a sufficient cut-off length, as suggested in Ansys (2022). When this condition was not met, they were modelled with shell elements as depicted in Fig. 2 for piping system Position #6.

Also, BFJs were the object of a comprehensive study due to their key role related to LoC. In more detail, the examined BFJs category consists of DN100-PN16 joints with a loose flange on one side and solid on the opposite, sealed by 8 bolts M16 and a 2 mm

	MESH SIZE	ELEMENT
a) Pipes	Hexahedral	5 mm SOLID186
b) Flanges	Tetrahedral	5 mm SOLID186
c) Gasket	Hexahedral	1 mm INTER195
d) Bolts-i.i.z.*	Tetrahedral	2 mm SOLID186
e) Bolts-o.i.z.*	Hexahedral	2 mm SOLID186
f) Welds	Tetrahedral	2 mm SOLID186

\* inside/outside influence zone

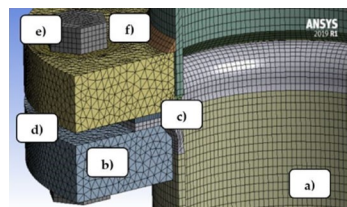


**Fig. 5** FE model discretization: **a** mesh size and element selected list; **b** mesh visualization and labels

aramid fibre gasket with NBR binder. To ensure leakage prevention, a minimum gasket pressure  $Q_{s,min}^L$  equal to 6 MPa is assigned, corresponding to  $L_{0,01}$  tightening class.

A refined FE model was developed in ANSYS (2022), to evaluate ultimate resistance and sealing performances. The model, depicted in Fig. 5b, takes into account contacts and material non-linearities through an appropriate nonlinear pressure-closure curve obtained in compliance with (Paolacci et al. 2021). Moreover, a refined meshing strategy was adopted: Table 5a and Fig. 5b summarize the salient features. In particular, pipes, flanges and bolts were discretized by quadratic brick elements SOLID186, due to irregularity geometry issues. Whilst for the gasket the INTER195 element was adopted, since it is specifically designed for flexible materials with primary deformation confined to the thickness direction.

Results of simulations are reported in Fig. 6. In greater detail, Fig. 6a represents the ultimate deformation exhibited by the joint in seismic conditions, whilst Fig. 6b depicts the ultimate strain levels. The analyses reveal a level of pressure distribution always less than the estimated  $Q_{s,min}^L$ , meaning no leakage could happen, as confirmed by visual inspection along the test campaign. Moreover, as a careful reader could notice, two considerations emerge from Fig. 6a, b that explained why leakage was hindered: (1) the exhibited significant rotation and (2) the higher slenderness of the collar resulted in additional prying forces, that inhibited the onset of leakage thanks to over-sealing performances. More precisely, the significant rotation of the loose flange, as can be noticed in Fig. 6a, generates a severe bending on the collar, leading to the formation of two plastic hinges. Thus, a plastic mechanism comparable to a T-Stub Mode 2 is developed. Hence, associated prying forces, due to the plastic mechanism, impose an additional gasket pressure at the external diameter: an extra-sealing performance, not considered by standard, is therefore triggered.

In addition, an enhanced analytical predictive model for leakage, thoroughly illustrated in UNI EN 1591-1 (2014), was adopted to understand LoC scenarios deeply. In detail, the analytical model results in an equivalent interaction shear on the loose flange  $F_L$  – axial  $F_{RI}$  forces leakage domain as shown in Fig. 7.

To be precise,  $F_{RI}$  is defined as the contribution of the load condition at stage *I* of the axial force and bending moment as  $F_{RI} = F_{AI} + 4M_{AI}/\phi$ , with  $\phi$  diameter of the pipe attached to the BFJ. According to the test scenarios, in the analytical model an internal pressure of 20 bar and a friction coefficient  $\mu=0.15$  were assumed. Therefore, in Fig. 7a, b, respectively, the leakage domains evaluated at SSE condition for both the MRF and BF configurations are illustrated. For both the analysed configurations, two domains

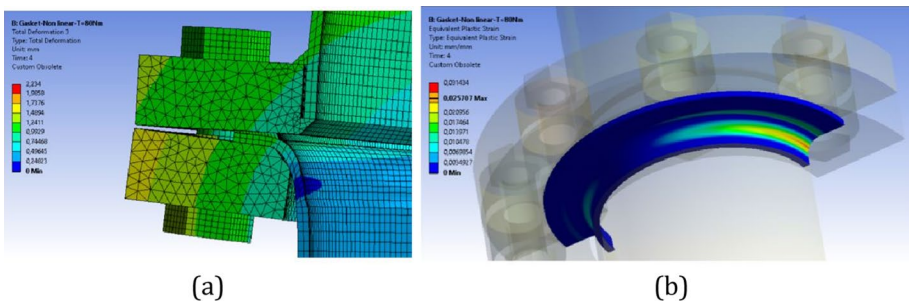
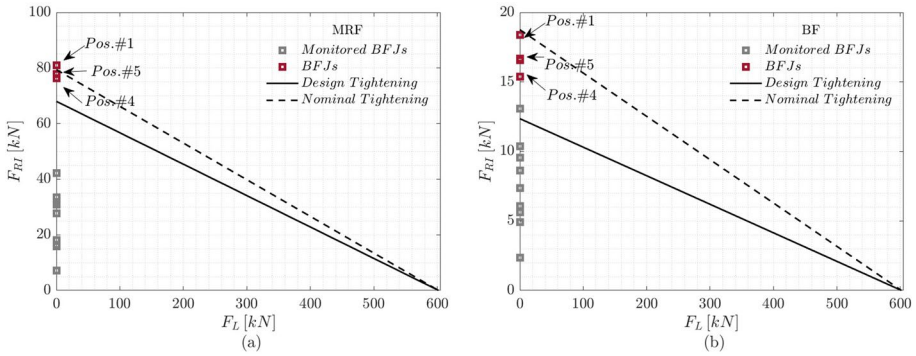


Fig. 6 FE model results via ANSYS<sup>®</sup> of BFJ: **a** deformation analysis; **b** strain analysis



**Fig. 7** Leakage predictions and interaction domains with and w.o. safety factors for SSE in **a** MRF and **b** BF configurations

were calculated: (1) one that considers safety factors associated to the adopted tightening technique, see Annex C and Annex F of European Committee for Standardization (2006), represented by the continuous black line; (2) one with nominal values related to the tightening effects, represented by the dashed line. Figure 7a, b collect predictions for all the installed BFJs on the two mock-up configurations. The red ones stand for the BFJs that were monitored along the test campaigns. Moreover, the initial tightening torque of  $80N \cdot m$  applied in the MRF configuration was loosened to  $40N \cdot m$  to simulate a possible maintenance issue effect. Once again, the predictions confirmed the experimental evidence: no leakage happened.

Finally, according to European Committee for Standardization (2006), it is possible to estimate axial, transversal and rotational stiffness parameters to apply to the equivalent simplified mechanical model of the BFJ. More precisely, they were evaluated in compliance with.

- Equation (48) §5.2 of Paolacci et al. (2021) for the axial stiffness:
- Tate and Rosenfeld formulation for the transversal stiffness  $1/K_s = 10t^3/24E_b I_b + 4t/3A_b G_b + 2tE_f/t^2 E_f^2$ ;
- by equilibrium considerations for the rotational stiffness:  $K_r = M_A/\phi_R = ded3eKa/8$ .

Last but not least, given the crucial function in the overall performance of the system, vertical and horizontal tanks have been thoroughly analysed.

As reported in Fig. 8, both high (HF) and low (LF) fidelity models were developed. In particular, the LF model results in a simplified stick model with an equivalent stiffness for each relevant degree of freedom that has been evaluated, i.e. two transversal and one torsional, and applied separately for each direction, as depicted in Fig. 8, based on modal characteristics and stiffness properties of the HF model. Concerning the HF, tanks were modelled by thick shell elements, assuming Mindlin-Reissner formulation. Moreover, as Fig. 8a–c indicated, a refined mesh is adopted near critical discontinuities, such as nozzles, BFJs connections and anchors. Steel grade class S235, with a damping ratio of 10%, according to nuclear standards, were assigned. To accurately evaluate the global seismic response and the seismic action effects on the supporting structure, it was assumed that the particulate contents move together with the tank shell with an effective mass estimated through the modelling updating (MU) technique, thoroughly discussed in the next Sect. 4.1.

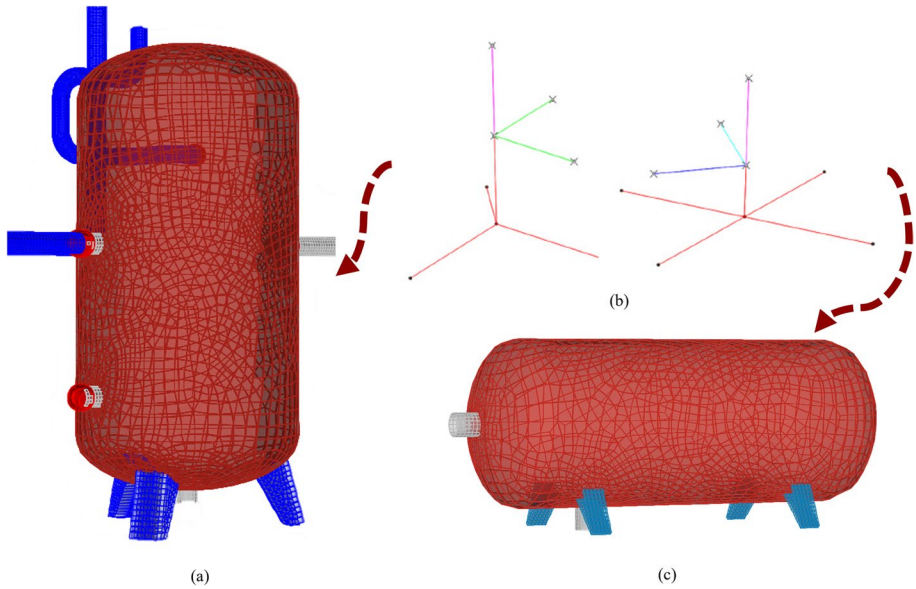


**Fig. 8** Local high fidelity models for **a** vertical and **c** horizontal tanks; **b** simplified stick models of the vertical and horizontal tanks

In more detail, 58% and 69% of participating mass of the total mass of the ensiled material were estimated by MU procedure for the MRF and the BF configurations, respectively.

Besides, to match the resulting stresses at the base tank footings, the residual masses, i.e.  $m_{res} = m_{tot} - m_{eff}$  the difference between the total ensiled granular masses and the participating seismic masses, were applied at the anchor levels. To capture the effects on the shell due to the response of the granular material to the seismic action, additional normal pressure on the wall.

$\Delta_{ph,s}$  was applied, according to:  $\Delta_{ph,s} = \alpha(z) \cdot \gamma \cdot \min(r_s^*; 3x) \cdot \cos \theta$ ; where  $x$  represents a vertical distance between a point on the tank’s wall and the apex of the hopper;  $\alpha(z)$  stands for the ratio of the response acceleration of the tank at a vertical distance  $z$  from the equivalent surface of the stored contents, to the acceleration of gravity;  $\gamma$  is the bulk unit weight of the stored granular material;  $r_s^* = \min(h_b, d_c/2)$ , where  $h_b$  is the overall height of the tank and  $d_c$  is the inside diameter;  $\theta$  is the angle between the radial line to the point of interest on the wall tank and the direction of the horizontal component of the seismic action, according to §3.3(6–8) (Bolstad 2010).

#### 4 Calibration and validation of the coupled structure-equipment model

The MRF and BF FE models were calibrated through a Bayesian model updating technique with the Metropolis–Hastings algorithm as a sampler. The implemented algorithm was devoted to matching the identified experimental frequencies and relevant mode shapes with the numerical ones. The validation was then pursued by comparing the acceleration time

histories at the floor levels and at the bottom of the vertical tanks of the FE models with the corresponding ones acquired by the accelerometers installed on the mock-up during the experimental test campaigns.

#### 4.1 Model calibration via Bayesian algorithm

Bayesian algorithms have received much interest in the field of FE model updating (FEMU), due to their flexibility. Developed on the basis of Bayes theorem, the main goal is to determine the posterior *pdf* of a set of parameters  $\theta$  given a set of  $\mathbf{y}$  observations/experimental data as illustrated in Eq. (1):

$$P(\theta|\mathbf{y}) \propto P(\mathbf{y}|\theta) \cdot P(\theta) \quad (1)$$

where  $P(\theta)$ ,  $P(\mathbf{y}|\theta)$ ,  $P(\theta|\mathbf{y})$  represents the prior distribution of  $\theta$ , the likelihood of the updating procedure and the posterior distribution of  $\theta$  conditioned by the experimental evidence.

The computational burden of Eq. (1) is mostly related to the complexity of the considered FE model and to the number of parameters that need to be updated. Besides, a close form or analytical solution for the posterior *pdf* is usually unavailable. Therefore, to draw samples from the posterior distribution, Monte Carlo (MC) algorithms are generally implemented. Among the MC methods, the Markov Chain MC (MCMC) methods (Hastings 1970) deserve mention. While classic MC methods proceed by drawing random samples independently from a fixed distribution, the MCMC instead draw samples from a proposal distribution, built on a Markov chain in which those candidate samples are either accepted or rejected as the new state of the chain. In this respect, the most adopted sampler algorithm is the Metropolis–Hastings (MH) (Boulkaibet et al. 2015), briefly sketched in the pseudo-code(1). The workflow begins with an initial guess  $\theta^0$  of the parameters set. Then, for  $N$  repetitions, a candidate  $\theta'$  state is sampled conditioned on the previous  $\theta^{(q-1)}$  set of parameters state. According to the MH algorithm, the new  $\theta'$  sample is either accepted or rejected according to the acceptance probability  $a_c$  evaluated as the ratio between the new posterior and the previous one. If  $a_c \geq u$ , where  $u$  is a random number sampled from a uniform distribution [0,1], then the new  $\theta'$  sample is accepted; otherwise, it is rejected and the next state is set equal to the previous one. Therefore, this procedure usually requires a huge number of iterations, with  $N \geq 10E4$ , to reach convergence for the parameters  $\theta$  distributions.

Hence, based on the results of global sensitivity analysis for both the SPIF MRF and BF mock-up, four parameters were drawn as the most informative for setting the model updating procedure. They were  $\theta_1$ , the steel structure Young modulus;  $\theta_2$  and  $\theta_3$  the seismic activated mass per meter and the effective height of the profile pressure of the ensiled granular material for the vertical tanks;  $\theta_4$  base joint stiffness. For the sake of clarity, from  $\theta_2$  and  $\theta_3$  can be calculated the % of effective participating seismic mass, as the ratio between the estimated experimental excited mass of the vertical tanks over the total mass ensiled, as defined in EN 1998:8-4 (Bolstad 2010). For  $\theta_1$  and  $\theta_4$ , according to the literature and common practice, Gaussian prior distributions were assigned, with the parameters defined in Tables 1 and 2 for the MRF and BF cases, respectively. Instead, due to the lack of information available for the

**Table 1** Probabilities density distributions of the updating parameters for the MRF configuration: prior and posterior parameters and type of distribution for each  $\theta_i$

			Prior PDF, Parameters	Posterior PDF, Parameters
$\theta_1$	Young Modulus	[GPa]	Gaussian, $\mu = 210; \sigma = 100$	Gaussian, $\mu = 220; \sigma = 50$
$\theta_2$	Part. mass of v.tanks	[ton/m]	Uniform, $a = 0; b = 1.22$	Gaussian, $\mu = 0.78; \sigma = 0.60$
$\theta_3$	H. of pressure profile	[m]	Uniform, $a = 0; b = 1.87$	Gaussian, $\mu = 0.25; \sigma = 0.1$
$\theta_4$	Base Joint stiffness	[MNm/rad]	Gaussian, $\mu = 20; \sigma = 5$	Gaussian, $\mu = 22.5; \sigma = 2.5$

**Table 2** Probabilities density distributions of the updating parameters for the BF configuration: prior and posterior parameters and type of distribution for each  $\theta_i$

			Prior PDF, Parameters	Posterior PDF, Parameters
$\theta_1$	Young Modulus	[GPa]	Gaussian, $\mu = 220; \sigma = 50$	Gaussian, $\mu = 219; \sigma = 30$
$\theta_2$	Part. mass of v.tanks	[ton/m]	Uniform, $a = 0; b = 1.22$	Gaussian, $\mu = 0.85; \sigma$
$\theta_3$	H. of pressure profile	[m]	Uniform, $a = 0; b = 1.87$	Gaussian, $\mu = 0.35; \sigma$
$\theta_4$	Base Joint stiffness	[MNm/rad]	Gaussian, $\mu = 22.5; \sigma = 5$	Gaussian, $\mu = 28.5; \sigma$

participating seismic masses described by  $\theta_2$  and  $\theta_3$  parameters, other than the recommendations reported in EN 1998:8–4 (U.S. Nuclear Regulatory Commission 2007), uniform distributions were assumed, as gathered in Tables 1 and 2 for the MRF and BF cases, respectively. In more detail, the standard in EN 1998:8-4 §3.3(4) recommends assuming 80% of the total mass of the granular content as effective mass applied in correspondence with the centre of gravity of the tank, in favour of safety and without more accurate studies.

**Algorithm 1** MH scheme

- 1: start with  $\theta^0$ , the first set of parameters
- 2: **for**  $q = 1, \dots, N$  **do**
- 3:     draw  $\theta'$  from a candidate density distribution  $p_c(\theta^{(q-1)}, \theta')$
- 4:     calculate the acceptance probability
 
$$a_c(\theta^{(q-1)}, \theta') = \min \left[ \frac{p(\theta' | \mathbf{y}) \cdot p_c(\theta^{(q-1)} | \theta')}{p_c(\theta^{(q-1)} | \mathbf{y}) \cdot p_c(\theta' | \theta^{(q-1)})} \right]$$
- 5:     draw  $u$ , a uniformly distributed random number  $\in [0, 1]$
- 6:
- 7:     **if**  $u \leq a_c$  **then**
- 8:          $\theta_q = \theta'$
- 9:     **else**
- 10:          $\theta_q = \theta^{(q-1)}$
- 11:     **end if**
- 12: **end for**

Hence, the likelihood, as in Mustafa and Matsumoto (2017), Das and Debnath (2018) and Zonta et al. (2014), for the MH procedure was set as a contribution of two terms: (1) the frequency error between the relevant experimental and numerical ones, described by a normal distribution; (2) the modal assurance criterion (MAC) mode shapes between experimental and FE modes, represented through a Beta distribution with  $\alpha = 5$ ,  $\beta = 0.5$  parameters. Moreover, to deal with the underflow numerical issues, the *log* formulation was adopted as reported in Eq. 2:

$$P(y|\theta) = \sum_{i=1}^4 \log \mathcal{N} \left( \left( \frac{f_{n_i}^{exp} - f_{n_i}^{FEM}}{f_{n_i}^{exp}} \right)^2, \mu_{fn}, \sigma_{fn}^2 \right) + - \sum_{i=1}^4 \log \mathcal{B}((1 - \text{diag}(\text{MAC}(\phi_i^{exp}, \phi_i^{FEM}))), \alpha, \beta) \tag{2}$$

The separated application of the algorithm to the MRF and BF cases for a total number of repetitions of 1E4 led to different posterior distributions for each parameter, shown in Tables 1 and 2, respectively. From the samples, posterior distributions were inferred via the maximum likelihood method. In particular, for the parameters  $\theta_1$  and  $\theta_4$  the inferred distributions are Gaussian, as the priors, with reduced dispersion. Instead, for the  $\theta_2$  and  $\theta_3$  parameters, the inferred posteriors are Gaussian distributions, deviating from the prior uniform distribution assumptions. This is strictly correlated to the definition of the likelihood that conditions the resampling. In fact, samples for which neither the error in frequency increases nor the MAC index decreases are excluded by the algorithm and, thus, the final distribution of the accepted samples follows a Gaussian distribution. It is worth noting that the posterior Gaussian distribution is truncated since it has to be defined within the physical limits of the parameters stated in the prior.

An additional remark regarding the seismic participating masses of the tanks deserves a mention. As anticipated in Sect. 3, a mismatch exists in terms of the estimated % participating mass of the FE models with reference to the safety recommendation of EN 1998:8-4 §3.3(4). In fact, whilst the standard recommends assuming 80% of the total mass of the granular content as effective mass, in favour of safety and without

**Table 3** Relevant model frequencies: numerical, i.e. evaluated through FE models; experimental, i.e. identified with rational fraction polynomials based on frequency response;  $\Delta$  percentage as  $(f_{n,exp} - f_{n,num})/f_{n,exp} \cdot 100$  for (a) the MRF and (b) the BF configurations

	Numerical [Hz]	Experimental [Hz]	$\Delta$ % [-]
<i>(a) MRF updated frequencies</i>			
$f_1$	2.81	2.88	2
$f_2$	4.84	4.24	- 14
$f_3$	6.73	6.38	- 5
$f_4$	9.18	8.95	- 5
	Numerical [Hz]	Experimental [Hz]	$\Delta$ % [-]
<i>(b) BF updated frequencies</i>			
$f_1$	4.54	4.50	- 1
$f_2$	6.36	6.83	7
$f_3$	7.94	7.84	- 1
$f_4$	9.91	10.04	1

more accurate studies, the results of the MU procedure yield instead to 58% and 69% values of participating seismic masses for the MRF and BF vertical tanks, respectively.

Finally, the predictive capabilities of the FE models, calibrated by assuming for the updating parameters the mean values of the posterior distributions, according to Cappello (2017) and Masi et al. (2019), have been checked with results stemming from the experimental frequencies. Tables 3a and 3b gather numerical FE and identified experimental frequencies for the MRF and BF mock-up, respectively. Thanks to the updating procedure, a good agreement for the most relevant frequencies of the system is achieved. In general, the results showed a very small percentage difference, except for only the second mode for the MRF. In this case, the difference between numerical and experimental recorded was 14%: this is related to the resonance effect between the second mode of the structure ( $\approx 4.80$  Hz) and the main period of the components ( $\approx 4.50$  Hz).

### 4.2 Model validation via nonlinear time history analyses

To assess the performance of the models in capturing the global behaviour and the dynamic interactions of the structures with the NSCs, a comparison between FE model results and those recorded during the experimental tests was conducted. Along this line and in view of the seismic risk assessment for the vertical tanks installed at the first level of the mock-ups, the acceleration time histories (THs) of the floor levels of the MRF and BF structures, together with the acceleration THs at the base level of the two vertical tanks were compared with the numerical ones. For the sake of brevity, only the THs plots of the first level of the structure and Tank #1 from the last test run of the experimental campaigns, corresponding to a seismic input with a PGA of 0.71 g for the MRF and 0.79 g for the BF, are gathered below.

Figures 9a, b gather the THs comparisons between the experimental and numerical results for the MRF configuration. The overall trend and response of the experimental THs are reflected in the numerical ones, especially in terms of peak values for the vertical tanks. Those are of utmost importance since they represent the EDP for the fragility assessment evaluated in Sect. 5. Similarly, Fig. 10a, b report the comparison between numerical and experimental THs of the first floor and of the base Tank #1 acceleration for the BF configuration. Anew, a good agreement between the general performance and maxima values is reached. In addition,

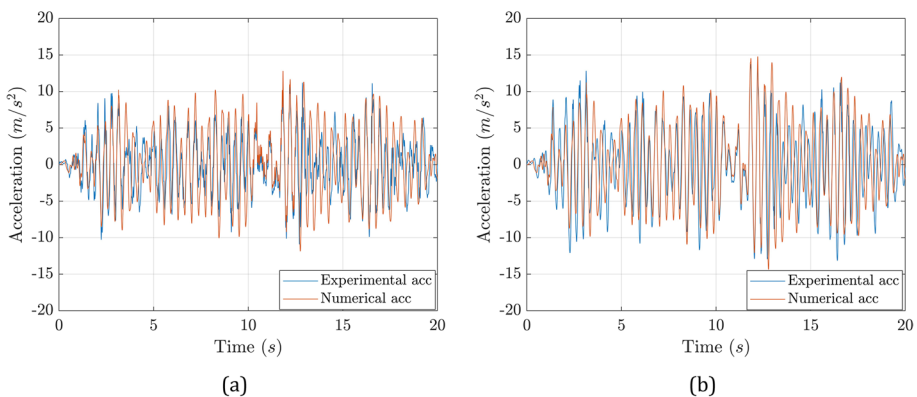


**Fig. 9** Numerical and experimental values: **a** acceleration TH at the 1st floor and **b** acceleration TH at the base level of Tank #1 for the MRF configuration

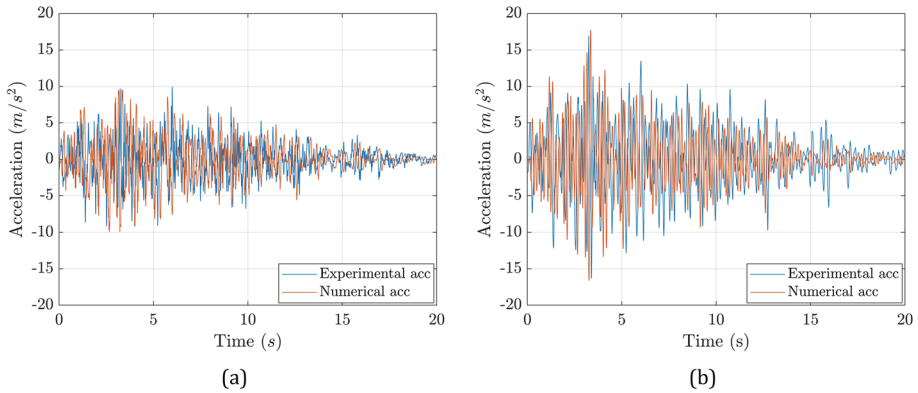


**Fig. 10** Numerical and experimental values: **a** acceleration TH at the 1st floor and **b** acceleration TH at the base level of Tank #1 for the BF configuration

a careful reader can notice by comparing the MRF and BF acceleration THs of floor response in Figs. 9a and 10a, that the MRF primary structure is more excited than the BF configuration, even though a higher seismic input was assigned to the MRF case. Instead, by comparing the acceleration THs of the base of the vertical Tank #1 in Figs. 9b and 10b, it emerges that the vertical Tank #1 in the BF configuration exhibits a higher peak acceleration value than the MRF case. This behaviour is strictly related to the dynamic properties of the coupled systems. As thoroughly analysed by the authors in Reza et al. (2014), the vertical tanks in the BF configuration acted as tuned mass dampers (TMDs), thus effectively limiting the accelerations to the structure, although a higher seismic input was assigned to the MRF case. Instead, the favourable effect of the TMD was not relevant for the MRF configuration.

Finally, the accuracy of the response of the whole FE models is quantitatively measured by means of the normalized energy error (NEE) defined as:

$$NEE(x_n, x_e) = \frac{\sum_{i=1}^n x_{n,i}^2 - \sum_{i=1}^n x_{e,i}^2}{\sum_{i=1}^n x_{n,i}^2} \tag{3}$$

where  $n$  represents the total length of the sampled THs,  $x_i$  and  $x_e$  stand for the numerical and experimental acceleration THs  $i$ -step values, respectively. Hence, for brevity, Table 4 gathers the NEE evaluated for the last run of the experimental campaigns—0.71 g for the MRF and 0.79 g for the BF—of the acceleration THs of the two vertical tanks at the base, for both the MRF and BF configurations. Good accuracy is achieved for both tanks involving NEE values within 7.5%.

**Table 4** NEE for acceleration THs of the last test run of the structure first floor and base level of the Tank #1 and Tank #2 for the MRF and the BF configuration

	NEE	
	MRF	BF
Tank #1	0.0748	0.0505
Tank #2	0.0653	0.0702

## 5 Seismic risk analysis of vertical tanks installed on industrial support structures

The risk assessment of the above-mentioned vertical Tank #1 and Tank #2 installed on the first floor of the SPIF mock-ups is presented and discussed hereinafter. To this end, a proper selection of seismic records becomes relevant. Hence, an innovative method for accelerogram selection developed by Giannini et al. (2022) was adopted. This methodology was applied in Butenweg et al. (2020) for the assessment of a 3D civil building, showing two main advantages: (1) it is no longer necessary to refer to a specific IM for the risk evaluation and (2) there is no need to perform any scaling operation on the selected accelerograms. Along these lines, this study aims to test the capability of the method also when applied to industrial process equipment, whose dependence on the frequency content of the earthquake may be significant. In this respect, two independent sets of 150 acceleration records, namely set A and set B, were cast using the aforementioned method; and the risk assessment is performed on the two vertical tanks of both MRF and BF configurations.

### 5.1 Input selection

To carry out risk analysis, the SPIF mock-ups were ideally located in the city of Amatrice, a small city of central Italy sadly known for the destructive 2016 Central Italy earthquake (Ministero delle infrastrutture e dei trasporti 2018). Amatrice is characterized by soil type B and belongs to the seismic zone 1, the most seismically vulnerable area according to the Italian national standard (Paolacci et al. 2022).

The seismic hazard of Amatrice was carried out by using a modified probabilistic seismic hazard analysis, formulated within the novel seismic risk framework proposed by Butenweg et al. (2020). In this respect, two independent sets of 150 accelerograms have been selected using the SCoReS Algorithm (Akkar and Bommer 2010), whose mean and mean+standard deviation well fit the corresponding median and 84% fractile uniform hazard reference spectra.

Five return periods were considered, i.e. 72, 224, 475, 975 and 2475 years, corresponding respectively to the probability of occurrence in 50 years of 50%, 20%, 10%, 5% and 2%. For each return period, thirty accelerograms were selected for each set, A and B, for a total of 300 natural records.

According to Butenweg et al. (2020), the hazard curve to be used for the risk assessment is derived using the mean value of the ground motion prediction equation (GMPE). In the present paper the GMPE of Hakkar and Bommer has been used, (Paolacci et al. 2022), whose corresponding hazard curve is illustrated in Fig. 11a.

The following parameters were taken into account for the record selection: magnitude range (4–8), fault-site distance range [0–100 km], ground type B, in agreement with the Italian Standard (Paolacci et al. 2022).

Figure 11b shows the mean and the mean+std response spectra of the 30 records compared with the corresponding median and 84% fractile target UHS. For brevity, only the spectra of the records selected for  $T_R = 475$  years are shown.

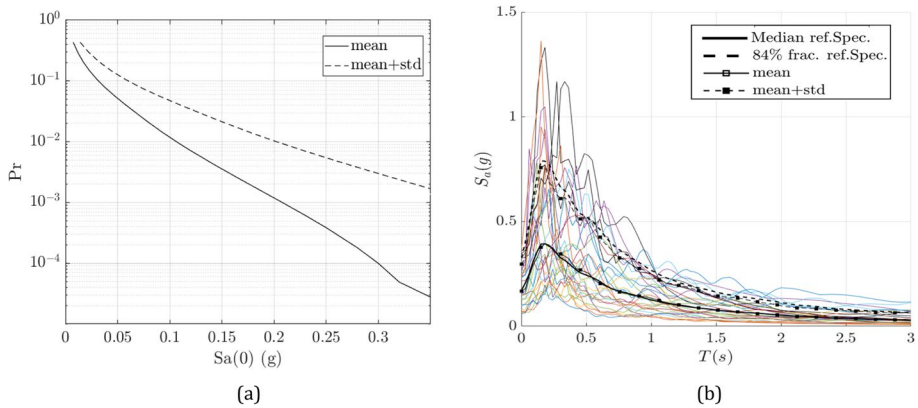


**Fig. 11** **a** Seismic hazard curves of Amatrice (Italy) and **b** Spectra of the 30 unscaled accelerograms selected for the hazard level  $T_R=475$  years, spectra of their logarithmic mean and the mean + 1 std compared with the target spectra

## 5.2 Fragility assessment

To perform risk assessment, it is necessary first to compute the vulnerability of the vertical tanks coupled with the global response of the MRF and BF systems, independently. According to the classic definition of fragility functions reported in Eq. 5, since fragilities estimate the EDP probability of exceedance of predefined thresholds, given a certain IM level, limit state levels, thresholds, EDPs and IMs must be defined.

More in detail, the peak ground acceleration (PGA) is considered as hazard parameter herein. It is worth noting that, due to the potentiality of the records selection method, this choice does not affect the risk assessment and it is necessary for the representation of the fragility curves only.

Instead, the relevant EDP for assessing the performances of the vertical tanks was identified in the maxima strain values recorded at the bottom wall-footing connections. Both the test campaign observations and the sensors data post-processing confirmed the connection of the bottom wall to the footing of the tanks as the weak link in the coupled support structure-tank system; also the results of a sensitivity analysis later on performed on the aforementioned local HF models presented in Sect. 3 indicate this critical region. However, there is a lack of standards and a limited amount of information on identifying reliable limit state thresholds related to storage tanks installed on support steel-rack systems, as investigated in the SPIF cases. In this regard, Vathi et al. (2017) identified performance criteria for the seismic design of industrial liquid storage tanks and piping systems, based on experimental observations and numerical data. In particular, related to unanchored (or self-anchored) storage tanks, the authors identify, as a general rule: (1) no damage below the steel yielding strain, e.g.  $\varepsilon_y \approx 1.3\%$ ; (2) limited or minor damage for  $\varepsilon_y < \varepsilon < 5\%$ , associated to a fit for service or DBE condition; (3) damage as soon as severe plasticization is reached, e.g. for strain level beyond  $5\%$ , denoting an SSE condition. Hence, to leverage and use the greatest number of experimental data available from the SPIF experimental campaigns, a linear regression model was set between the maximum acceleration  $\max(|acc|)$  recorded at the base of the vertical tanks and the maximum strains  $\max(|\varepsilon|)$  recorded at the bottom wall

of the tank and its footing connection. The procedure was repeated for each shake table test run performed for the BF case since strain data availability was assured only for this configuration. The regression model depicted in Fig. 12b is described as,

$$\epsilon = p_1 \cdot acc + p_2 \tag{4}$$

where  $acc$  is associated with  $\mu=10.96 \text{ m/s}^2$  and  $\sigma=4.139 \text{ m/s}^2$ ; whilst for the  $p_i$  coefficients with 95% confidence bounds hold  $p_1=0.6441$  (0.5665, 0.7218) and  $p_2=1.107$  (1.035, 1.179), with high goodness of fit indices, e.g. sum of squared error=0.0274 and  $R^2=0.9891$ , respectively.

The regression reported in Fig. 12b indicated that up to the test RUN #5, the strain histories plotted in Fig. 12a recorded values below the  $\epsilon_y$  threshold; whilst at the test RUN #7, i.e. the last one, local plasticization was detected by the sensors. Therefore, in compliance with the indications found in the literature, data confirmed a fit for service limit state until test RUN #5 and the SSE state beyond test RUN #7. Thus, from the regression model, the accelerations identified by threshold strain value are derived:  $10 \text{ m/s}^2$  and  $16 \text{ m/s}^2$  as DBE and SSE limit states, respectively.

Then, for both the DBE and SSE limit states, fragility functions are evaluated, based on the log-normal distribution hypothesis,

$$P(D|IM = y) = \Phi\left(\frac{\log(y/\theta)}{\beta}\right) \tag{5}$$

where  $P(D|IM=y)$  defines the probability that a ground motion with  $IM=y$  will cause the structure to reach a certain damage level D;  $\Phi(\cdot)$  is the standard normal cumulative distribution function (CDF);  $\theta$  is the median of the fragility function and  $\beta$  is the standard deviation of  $\log IM$ .

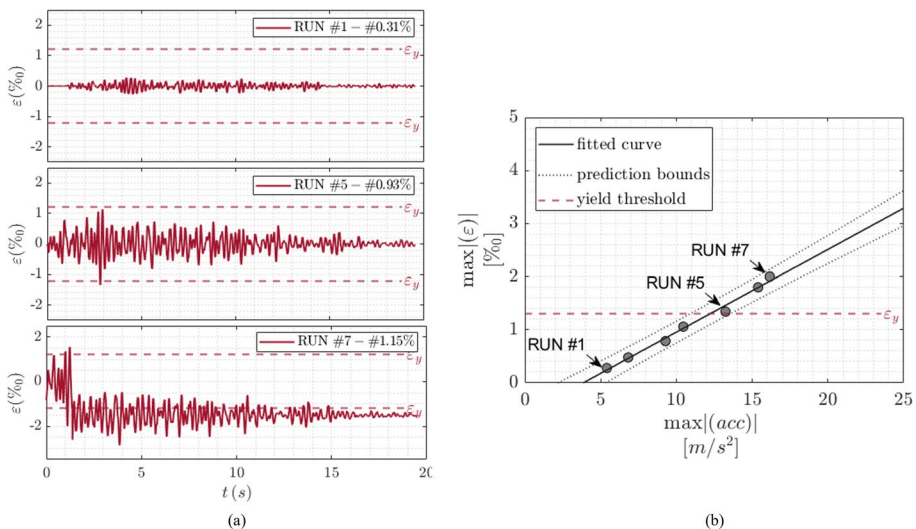


**Fig. 12** **a** THs of strains for test RUN #1, #5 and #7 recorded at the bottom wall-tank footing connection of the vertical Tank #1 installed at the 1<sup>st</sup> floor with the  $\epsilon_y$  thresholds highlighted; **b** maxima bottom-wall strain and acceleration experimental measures for Tank #1 collected during the BF experimental test campaign and linear regression model with confidence bounds of 95%

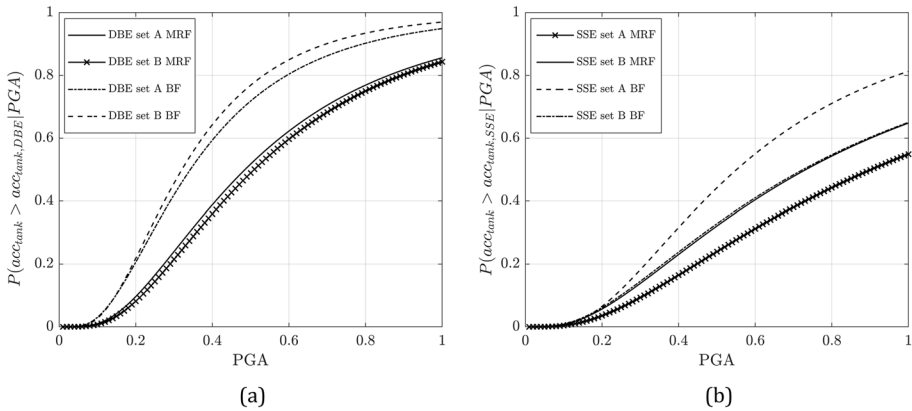


**Fig. 13** **a** Tank #1 fragility curves for DBE for MRF and BF set A and set B **b** Tank #1 fragility curves for SSE for MRF and BF set A and set B

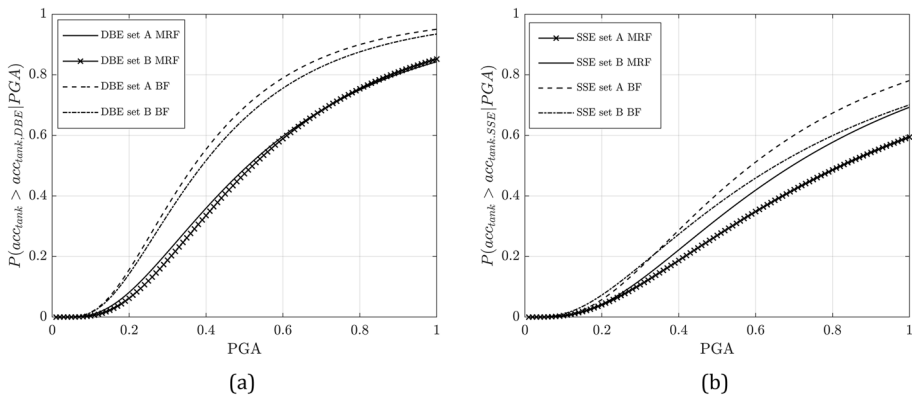


**Fig. 14** **a** Tank #2 fragility curves for DBE for MRF and BF set A and set B **b** Tank #2 fragility curves for SSE for MRF and BF set A and set B

### 5.3 Risk assessment and discussion of the results

To quantify the risk assessment of the of the two vertical tanks installed at the 1st floor, the MAF is evaluated both for the DBE and SSE limit states, as the convolution described here:

$$\lambda(D) = \int P(D|IM = y) d\lambda(y) \tag{6}$$

in which  $\lambda(y)$  represents the mean annual rate of exceedance of the seismic hazard and  $P(D|IM=y)$  defines the fragility function defined in (5). Figures 13a and 14a depict the fragility curves, related to the DBE limit state, of the two vertical tanks for both the BF and MRF configurations. The curves refer to the two sets of selected accelerograms, i.e. set A and set B; likewise, Figs. 13b and 14b show the fragility assessment for the SSE limit state. A careful reader can notice that the vulnerability of the NSCs is higher in the

**Table 5** Mean annual frequency of exceedance for (a) at DBE and (b) SSE limit state conditions for Tank #1

	DBE	
	Set A	Set B
(a)		
MRF	0.00027	0.00024
BF	0.00054	0.00053
	SSE	
	Set A	Set B
(b)		
MRF	0.00012	0.00014
BF	0.00013	0.00015

BF configuration for both the limit states considered. These differences are more evident in the DBE limit state, while they are noticeable in the SSE limit state for PGA values higher than 0.2 g, due to the higher EDP threshold that cannot be reached with low PGA values. These results agree with the experimental evidence described in Reza et al. (2014), where the dynamic interaction between the primary structure and the secondary elements demonstrated a higher seismic response for the vertical tanks on the first floor of the BF configuration due to their TMD effects. Furthermore, if one focuses on the influence of the two sets for assessing the fragility of each configuration, it can be noticed that they are very close for the two selected sets. This is especially true for the DBE limit state as shown in Figs. 13a and 14a. The corresponding differences in fragilities that appear in Figs. 13b and 14b for the SSE, could be reduced by increasing the number of selected accelerograms; nonetheless, this increase has not been pursued further given the negligible influence on the corresponding MAFs evaluated herein. Eventually, the integration of the fragility curves of the NSCs with the hazard curve of the site via Eq. (6) entails the MAF of occurrence for both limit states and accelerogram sets. Tables 5(a) and 6(a) collect the values of MAF for the DBE limit states for both set A and set B, whilst the SSE results are gathered in

**Table 6** Mean annual frequency of exceedance for (a) at DBE and (b) SSE limit state conditions for Tank #2

	DBE	
	Set A	Set B
(a)		
MRF	0.00022	0.00019
BF	0.00050	0.00051
	SSE	
	Set A	Set B
(b)		
MRF	0.00012	0.00011
BF	0.00010	0.00012

Tables 5(b) and 6(b). The high value of the DBE risk index of the tanks in the BF configuration is clear. Conversely, the aforementioned difference in vulnerability between the two configurations does not hold for the SSE risk index, where similar values are involved. The underlying reason is related to the seismic hazard level of the site. As a matter of fact, see Fig. 11a, the hazard curve shows a relatively low probability value for the site with PGA higher than 0.3 g where the difference of the vulnerability for the SSE is more evident, see Fig. 13b and, therefore, its contribution in the MAF evaluation is negligible. In sum, the risk indices values associated with set A or set B approach the same values for both the analysed configuration. Therefore, the independence of the seismic risk assessment from the selected accelerogram sets pointed out in Butenweg et al. (2020) is also verified in this application which involves NSCs.

## 6 Conclusions and future developments

This study aimed to investigate the seismic risk assessment of two coupled structure-secondary equipment systems involving heavy vertical tanks; it was based on experimental data derived from an extensive full-scale testing campaign conducted on a shaking table. To guide the experimental tests, efficient FE models were developed that were reliable on the one hand and accurate, on the other hand, to the point of being able to capture the complex dynamic interaction between the main structure and non structural components (NCs), which characterises this type of systems. In particular, attention was paid to the computational burden associated to the FE models; and, in the framework of performance-based earthquake engineering (PBEE), for a practical seismic risk assessment a good trade-off between computational burden and model complexity must be found.

Moreover, to significantly reduce the long-standing problem associated with the record-to-record variability for the selection of input sets for seismic risk assessment, an innovative seismic record selection algorithm was used. Its efficiency was tested on the two first-floor vertical tanks, which were highly dependent on the multi-modal and high-frequency response of the coupled systems. For this purpose, two different sets of 150 accelerograms were selected. The results obtained from the analyses conducted on the two sets were then compared in terms of both vulnerability and risk.

Along these veins, the proposed study has examined the design and performances of a 3D FE model validated against data acquired during shake table tests of the real mock-ups. The rationale behind the implementation of the FE models relies on finding an optimum between accuracy and fidelity to the experimental data and the computational burden required by several runs of a relatively accurate 3D FE model. On these premises, the strategy adopted in modelling involves the development of speedy and simplified global models. The simplification stems from a condensation of the degree of complexity of the problem through the separate development of: (1) analytical models, such as for the BFJs' leakage domain; (2) stick models, such as those for tanks; (3) equivalent stiffnesses, such as those for base joint springs. In this fashion, the global 3D FE model was enriched with information from local high-fidelity models. This reduces the entire calculation burden from, for instance, the seismic analysis of a single BFJ of  $\approx 9$  h, to an overall seismic simulation run time of the global model of only a few minutes. The time factor certainly plays a key role in the PBEE for the possibility of conducting risk analyses. The FE models set have revealed a good capability to catch the seismic behaviour of the NSCs, especially for the maximum acceleration value measured on the tanks. This has demonstrated that,

paying the right attention to the modelling of significant local behaviors, it is possible to obtain good predictions with sound FEM models.

The seismic risk assessment conducted with the aforementioned calibrated models has highlighted the influence of the dynamic interaction between the primary structure and the installed vertical tanks, as already highlighted by the experimental campaign. Therefore, owing to the explored dynamical properties and the TMD effects, the results demonstrated the higher vulnerability of the tanks located on the BF structure with respect to those of the MRF structure. Finally, the application of the new methodology for the selection of a set of ground motions demonstrated its efficiency by entailing close indices for vulnerability and risk assessment. As such, the methodology ensures the independence of risk evaluations from the adopted set of accelerograms: an undoubted advantage for researchers and designers. Further analyses on other NSCs are needed for reliability evaluations. In this context, surrogate modelling and machine learning techniques may further mitigate the computational time involved.

**Acknowledgements** The research leading to these results has received funding from the European Community's HORIZON 2020 Framework Programme [H2020-INFRAIA2016-2017/H2020-INFRAIA-2016-1] for access to the EUCENTRE Laboratory under grant agreement n° 730900—SERA project. The second and the last author acknowledge the Italian Ministry of Education, Universities and Research (MUR) in the framework of the project PNRR CN ICSC Spoke 9 and DICAM-EXC (*Departments of Excellence 2023–2027*, grant L232/2016), respectively.

**Funding** Open access funding provided by Università degli Studi Roma Tre within the CRUI-CARE Agreement.

## Declarations

**Conflict of interest** The authors declare that they have no conflict of interest.

**Open Access** This article is licensed under a Creative Commons Attribution 4.0 International License, which permits use, sharing, adaptation, distribution and reproduction in any medium or format, as long as you give appropriate credit to the original author(s) and the source, provide a link to the Creative Commons licence, and indicate if changes were made. The images or other third party material in this article are included in the article's Creative Commons licence, unless indicated otherwise in a credit line to the material. If material is not included in the article's Creative Commons licence and your intended use is not permitted by statutory regulation or exceeds the permitted use, you will need to obtain permission directly from the copyright holder. To view a copy of this licence, visit <http://creativecommons.org/licenses/by/4.0/>.

## References

- Akkar S, Bommer J (2010) Empirical equations for the prediction of PGA, PGV, and spectral accelerations in Europe, the mediterranean region, and the middle east. *Seismol Res Lett* 81:195–206. <https://doi.org/10.1785/gssrl.81.2.195>
- Alessandri S, Caputo AC, Corritore D, Giannini R, Paolacci F, Phan HN (2018) Probabilistic risk analysis of process plants under seismic loading based on Monte Carlo simulations. *J Loss Prev Process Ind* 53:136–148. <https://doi.org/10.1016/j.jlp.2017.12.013>
- American Society of Mechanical Engineering (2000) B31.3: process piping
- Ansys (2022) Academic research mechanical, release 18.1
- ASCE/SEI (2016) Minimum design loads and associated criteria for buildings and other structures
- Azizpour O, Hosseini M (2009) A verification study of ASCE recommended guidelines for seismic evaluation and design of “on pipe-way piping” in petrochemical plants, pp 1–10. [https://doi.org/10.1061/41050\(357\)33](https://doi.org/10.1061/41050(357)33)
- Bertero RD, Bertero VV (2002) Performance-based seismic engineering: the need for a reliable conceptual comprehensive approach. *Earthq Eng Struct Dyn* 31(3):627–652. <https://doi.org/10.1002/eqe.146>

- Bolstad WM (2010) Understanding computational bayesian statistics
- Boulkaibet I, Mthembu L, Marwala T, Friswell M, Adhikari S (2015) Finite element model updating using an evolutionary Markov chain Monte Carlo algorithm, vol 2. [https://doi.org/10.1007/978-3-319-15248-6\\_26](https://doi.org/10.1007/978-3-319-15248-6_26)
- Bursi OS, Reza MS, Abbiati G, Paolacci F (2015) Performance-based earthquake evaluation of a full-scale petrochemical piping system. *J Loss Prev Process Ind* 33:10–22. <https://doi.org/10.1016/j.jlp.2014.11.004>
- Bursi OS, Paolacci F, Reza MS, Alessandri S, Tondini N (2016) Seismic assessment of petrochemical piping systems using a performance-based approach. *J Press Vessel Technol* 138:3. <https://doi.org/10.1115/1.4032111>
- Butenweg C, Bursi OS, Paolacci F, Marinkovic M, Lanese I, Nardin C, Quinci G (2021) Seismic performance of an industrial multi-storey frame structure with process equipment subjected to shake table testing. *Eng Struct*. <https://doi.org/10.1016/j.engstruct.2021.112681>
- Butenweg C et al (2020) Seismic performance of multi-component systems in special risk industrial facilities, Tech. rep., Deliverable D10.1, SERA Project, Project. No: 730900, H2020-EU – Seismology and Earthquake Engineering Research Infrastructure Alliance for Europe
- Calvi PM, Sullivan TJ (2014) Estimating floor spectra in multiple degree of freedom systems. *Earthq Struct* 7:17–38
- Cappello C (2017) Theory of decision based on structural health monitoring. PhD thesis, University of Trento, Italy
- Caputo A, Paolacci F, Bursi O, Giannini R (2019) Problems and perspectives in seismic quantitative risk analysis of chemical process plants. *J Pressure Vessel Technol Trans ASME*. <https://doi.org/10.1115/1.4040804>
- Caputo A, Kalemi B, Corritore D, Paolacci F (2020) Computing resilience of process plants under Na-tech events: methodology and application to seismic loading scenarios. *Reliab Eng Syst Safety* 195. <https://doi.org/10.1016/j.ress.2019.10668>
- Das A, Debnath N (2018) A bayesian finite element model updating with combined normal and lognormal probability distributions using modal measurements. *Appl Math Model* 61:457–483. <https://doi.org/10.1016/j.apm.2018.05.004>
- De Angelis M, Giannini R, Paolacci F (2010) Experimental investigation on the seismic response of a steel liquid storage tank equipped with floating roof by shaking table tests. *Earthq Eng Struct Dyn* 39(4):377–396. <https://doi.org/10.1002/eqe.945>
- Di Sarno L, Karagiannakis G (2020) On the seismic fragility of pipe rack—piping systems considering soil–structure interaction. *Bull Earthq Eng* 18:2723–2757. <https://doi.org/10.1007/s10518-020-00797-0>
- European Committee for Standardization (2005) Eurocode 3—design of steel structures—part 1–8: design of joints
- European Committee for Standardization (2004) Eurocode 8—part 4: silos, tanks and pipelines
- European Committee for Standardization (2006) Design of structures for earthquake resistance. Eurocode 8–4: Silos, tanks and pipelines. CEN/TC 250, Brussels
- European Committee for Standardization (2011) Metallic industrial piping—part 3: design and calculation. EN 13480-3
- Giannini R, Paolacci F, Phan HN, Corritore D, Quinci G (2022) A novel framework for seismic risk assessment of structures. *Earthq Eng Struct Dyn* 51(14):3416–3433. <https://doi.org/10.1002/eqe.3729>
- Hastings WK (1970) Monte Carlo sampling methods using Markov chains and their applications. *Biometrika* 57:24
- IDEA (2022) Statica: steel-v.10.1
- Kireev O, Berkovsky A (2013) Parametric study of flexibility factor for curved pipe and welding elbows
- Masi A, Chiauzzi L, Santarsiero G (2019) Seismic response of RC buildings during the Mw 6.0 August 24, 2016 Central Italy earthquake: the Amatrice case study. *Bull Earthq Eng* 17:5631–5654
- Merino Vela RJ, Brunesi E, Nascimbene R (2018) Floor spectra estimates for an industrial special concentrically braced frame structure. *J Pressure Vessel Technol*. <https://doi.org/10.1115/1.4041285>
- Merino RJ, Brunesi E, Nascimbene R (2019) Seismic assessment of an industrial frame-tank system: development of fragility functions. *Bull Earthq Eng* 17:2569–2602. <https://doi.org/10.1007/s10518-018-00548-2>
- Ministero delle Infrastrutture e dei Trasporti (2018) NTC 18 Norme Tecniche per le costruzioni. Gazzetta ufficiale della Repubblica Italiana
- Mustafa S, Matsumoto Y (2017) Bayesian model updating and its limitations for detecting local damage of an existing truss bridge. *J Bridge Eng*. [https://doi.org/10.1061/\(ASCE\)BE.1943-5592.0001044](https://doi.org/10.1061/(ASCE)BE.1943-5592.0001044)

- Nardin C, Bursi OS, Paolacci F, Pavese A, Quinci G (2022) Experimental performance of a multi-storey braced frame structure with non-structural industrial components subjected to synthetic ground motions. *Earthq Eng Struct Dyn*. <https://doi.org/10.1002/eqe.3656>
- Necci A, Cozzani V, Spadoni G, Khan F (2015) Assessment of domino effect: state of the art and research needs. *Reliab Eng Syst Saf* 143:3–18. <https://doi.org/10.1016/j.res.2015.05.017>
- Paolacci F, Quinci G, Nardin C, Vezzari V, Marino A, Ciucci M (2021) Bolted flange joints equipped with FBG sensors in industrial piping systems subjected to seismic loads. *J Loss Prev Process Ind* 72. <https://doi.org/10.1016/j.jlp.2021.104576>
- Paolacci F, Giannini R, Quinci G (2022) Scores: an algorithm for records selection to employ in seismic risk and resilience analysis. XIX Convegno ANIDIS L'ingegneria Sismica in Italia, Torino, 11–15 settembre 2022
- Reza MS, Bursi OS, Paolacci F, Kumar A (2014) Enhanced seismic performance of non-standard bolted flange joints for petrochemical piping systems. *J Loss Prev Process Ind* 30:124–136. <https://doi.org/10.1016/j.jlp.2014.05.011>
- SAP2000-v22 (2022) Structural analysis and design. CSI Computer and Structures, Inc.
- Sayginer O, di Filippo R, Lecoq A, Marino A, Bursi OS (2020) Seismic vulnerability analysis of a coupled tank-piping system by means of hybrid simulation and acoustic emission. *Exp Tech* 44:807–819. <https://doi.org/10.1007/s40799-020-00396-3>
- U.S. Nuclear Regulatory Commission (2007) Regulatory guide 1.61, damping values for seismic design of nuclear power plants
- UNI EN 1591-1 (2014) Design rules for a gasketed circular flange connection—part 1: calculation method
- UNI EN 13555 (2021) Flanges and their joints—gasket parameters and test procedures relevant to the design rules for gasketed circular flange connections
- Vathi M, Karamanos S, Kapogiannis I, Spiliopoulos K (2017) Performance criteria for liquid storage tanks and piping systems subjected to seismic loading. *J Pressure Vessel Technol*. <https://doi.org/10.1115/1.4036916>
- Zito M, Nascimbene R, Dubini P, D'Angela D, Magliulo G (1871) Experimental seismic assessment of nonstructural elements: testing protocols and novel perspectives. *Buildings* 2022:12. <https://doi.org/10.3390/buildings12111871>
- Zonta D, Bruschetta F, Cappello C, Zandonini R, Pozzi M, Wang M, Glisic B, Inaudi D, Posenato D, Zhao Y (2014) On estimating the accuracy of monitoring methods using bayesian error propagation technique, vol 9061. <https://doi.org/10.1117/12.2046409>

**Publisher's Note** Springer Nature remains neutral with regard to jurisdictional claims in published maps and institutional affiliations.

## Authors and Affiliations

Gianluca Quinci<sup>1</sup> · Chiara Nardin<sup>2</sup> · Fabrizio Paolacci<sup>1</sup>  · Oreste S. Bursi<sup>2</sup>

✉ Fabrizio Paolacci  
fabrizio.paolacci@uniroma3.it

Gianluca Quinci  
gianluca.quinci@uniroma3.it

Chiara Nardin  
chiara.nardin@unitn.it

Oreste S. Bursi  
oreste.bursi@unitn.it

<sup>1</sup> Department of Civil, Computer Science and Aeronautical Technologies Engineering, Roma Tre University, Via Vito Volterra 62, 00146 Rome, Italy

<sup>2</sup> Department of Civil, Environmental and Mechanical Engineering, University of Trento, Via Mesiano 77, 38123 Trento, Italy